UC Irvine
UC Irvine Previously Published Works

Title
Chemical characterization of water-soluble organic carbon aerosols at a rural site in the Pearl River Delta, China, in the summer of 2006

Permalink
https://escholarship.org/uc/item/9v0354mr

Journal
Journal of Geophysical Research, 114(D14)

ISSN
0148-0227

Authors
Miyazaki, Y
Kondo, Y
Shiraiwa, M
et al.

Publication Date
2009

DOI
10.1029/2009jd011736

Copyright Information
This work is made available under the terms of a Creative Commons Attribution License, availalbe at https://creativecommons.org/licenses/by/4.0/

Peer reviewed

eScholarship.org Powered by the California Digital Library
University of California

Chemical characterization of water-soluble organic carbon aerosols at a rural site in the Pearl River Delta, China, in the summer of 2006

Y. Miyazaki,[1,2] Y. Kondo,[1] M. Shiraiwa,[1,3] N. Takegawa,[1] T. Miyakawa,[1] S. Han,[1] K. Kita,[4] M. Hu,[5] Z. Q. Deng,[5] Y. Zhao,[6] N. Sugimoto,[7] D. R. Blake,[8] and R. J. Weber[9]

Received 9 January 2009; revised 6 May 2009; accepted 26 May 2009; published 31 July 2009.

[1] Online measurements of water-soluble organic carbon (WSOC) aerosols were made using a particle-into-liquid sampler (PILS) combined with a total organic carbon (TOC) analyzer at a rural site in the Pearl River Delta region, China, in July 2006. A macroporous nonionic (DAX-8) resin was used to quantify hydrophilic and hydrophobic WSOC, which are defined as the fractions of WSOC that penetrated through and retained on the DAX-8 column, respectively. Laboratory calibrations showed that hydrophilic WSOC ($WSOC_{HPI}$) included low-molecular aliphatic dicarboxylic acids and carbonyls, saccharides, and amines, while hydrophobic WSOC ($WSOC_{HPO}$) included longer-chain aliphatic dicarboxylic acids and carbonyls, aromatic acids, phenols, organic nitrates, cyclic acids, and fulvic acids. On average, total WSOC (TWSOC) accounted for 60% of OC, and $WSOC_{HPO}$ accounted for 60% of TWSOC. Both $WSOC_{HPI}$ and $WSOC_{HPO}$ increased with photochemical aging determined from the NO_x/NO_y ratio. In particular, the average $WSOC_{HPO}$ mass was found to increase by a factor of five within a timescale of ~10 hours, which was substantially larger than that of $WSOC_{HPI}$ (by a factor of 2–3). The total increase in OC mass with photochemical aging was associated with the large increase in $WSOC_{HPO}$ mass. These results, combined with the laboratory calibrations, suggest that significant amounts of hydrophobic organic compounds (likely containing large carbon numbers) were produced by photochemical processing. By contrast, water-insoluble OC (WIOC) mass did not exhibit significant changes with photochemical aging, suggesting that chemical transformation of WIOC to WSOC was not a dominant process for the production of WSOC during the study period.

Citation: Miyazaki, Y., et al. (2009), Chemical characterization of water-soluble organic carbon aerosols at a rural site in the Pearl River Delta, China, in the summer of 2006, *J. Geophys. Res.*, *114*, D14208, doi:10.1029/2009JD011736.

1. Introduction

[2] Water-soluble organic carbon (WSOC) can significantly alter the hygroscopicity of aerosols and can be important in determining the ability of particles to act as cloud condensation nuclei (CCN) [*Novakov and Penner*, 1993; *Saxena et al.*, 1995; *Facchini et al.*, 1999]. A major source of WSOC is considered to be secondary organic aerosols (SOA), formed by the oxidation of volatile organic compounds (VOCs) followed by condensation on existing particles and/or nucleation. Recent field studies have shown that bulk WSOC and estimated SOA had similar chemical characteristics in an urban area [*Miyazaki et al.*, 2006; *Kondo et al.*, 2007], pointing to the potential role of WSOC measurements in tracing SOA formation. Over regions remote from primary sources, WSOC also includes aged primary components of organic carbon (OC) as well as SOA [*Fuzzi et al.*, 2006], and thus accounts for a significant portion of the OC mass.

[3] In a broad definition, WSOC can be classified into hydrophilic (more soluble in water) and hydrophobic (less soluble in water) fractions [*Duarte and Duarte*, 2005; *Sullivan and Weber*, 2006]. While the definitions of these fractions are operational, they are closely related to the carbon chain length and number of functional groups per molecule. Hydrophilic organic compounds are highly oxygenated, with low molecular weights, typically with a number of carboxyl, carbonyl, or other groups per molecule. These compounds tend to be highly soluble in water. Hydro-

[1]Research Center for Advanced Science and Technology, University of Tokyo, Tokyo, Japan.
[2]Now at Institute of Low Temperature Science, Hokkaido University, Sapporo, Japan.
[3]Now at Biogeochemistry Department, Max Planck Institute for Chemistry, Mainz, Germany.
[4]Department of Environmental Science, Ibaraki University, Ibaraki, Japan.
[5]State Key Joint Laboratory of Environmental Simulation and Pollution Control, College of Environmental Sciences and Engineering, Peking University, Beijing, China.
[6]Air Quality Research Center, University of California, Davis, California, USA.
[7]National Institute for Environmental Studies, Tsukuba, Japan.
[8]Department of Chemistry, University of California, Irvine, California, USA.
[9]School of Earth and Atmospheric Sciences, Georgia Institute of Technology, Atlanta, Georgia, USA.

Copyright 2009 by the American Geophysical Union.
0148-0227/09/2009JD011736

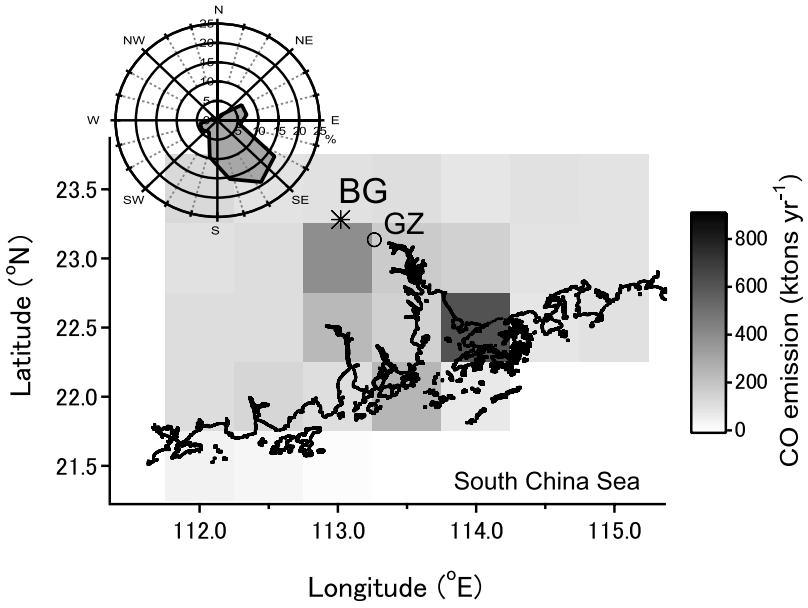

Figure 1. Location of the sampling site (BG, backyard garden) and the observed frequency of the local wind direction with wind speed >1 m s^{-1}. GZ indicates the location of urban Guangzhou. Distributions of anthropogenic emissions of CO for the year 2006 at 0.5° × 0.5° resolution [*Zhang et al.*, 2009] are also shown.

phobic organic compounds tend to be longer in carbon chain length, and less hygroscopic. An important class of hydrophobic WSOC is humic-like substances (HULIS). These are a mixture of high-molecular-weight compounds that are strong surfactants [*Decesari et al.*, 2000], which could decrease surface tension of aerosol and fog water [*Facchini et al.*, 2000; *Kiss et al.*, 2005]. Despite their importance, their sources and formation process remain poorly understood. Consequently, chemical transformations that may affect organic aerosol composition during air-mass aging need to be investigated.

[4] As a huge continental aerosol source region, the Pearl River Delta (PRD), with an area of about 4.2×10^4 km^2, is located in southern China, extending from the Hong Kong metropolitan area to the northwest. The PRD surrounds 14 cities and countries in Guangdong Province. Guangdong Province is one of the fastest growing economic centers in China and 40–50 million people live in the PRD region. Previous studies on the chemical analysis of organic compounds in the PRD region have been made primarily at urban sites, in Hong Kong and Guangzhou [e.g., *Zheng et al.*, 1997; *Feng et al.*, 2006]. Most of these studies identified solvent-extractable OC, including *n*-alkanes, polycyclic aromatic hydrocarbons, *n*-fatty acids, *n*-alkanols and dicarboxylic acids, mainly from the viewpoint of source identification. These identified compounds accounted for only <10% of the total OC. *Andreae et al.* [2008] reported aerosol light absorption in urban Guangzhou and suggested that substantial contributions of OC were required to explain the observed light absorption (either by light absorption by OC, or by internal mixing between OC and EC).

[5] Semicontinuous measurements of chemically fractionated organic aerosols according to their water solubility were made in July 2006 at a rural site in the PRD region of south China. This field study was part of the Program of Regional Integrated Experiments of Air Quality over the PRD (PRIDE-PRD) campaign, 2006. This study presents results of time-resolved measurements of bulk and chemically fractionated (hydrophilic and hydrophobic) WSOC, using a macroporous nonionic (DAX-8) resin. In particular, the dependence of the fractionated WSOC on photochemical aging is discussed.

2. Experiments

[6] Measurements were made on the top floor of a building (~15 m above ground level) in the Backyard Garden (BG) at a rural site (23.28°N, 113.02°E) located ~50 km northwest of urban Guangzhou in the PRD, China. The location of the sampling site and the surrounding area are shown in Figure 1. Ambient air was sampled from the rooftop of the building. The sample line from the inlet on the rooftop to each instrument was a 6-m-long stainless and copper tube, with a 1-cm inner diameter. Simultaneous measurements of aerosol chemical compositions and gas species were made during 6–31 July 2006.

2.1. Total and Isolated WSOC

[7] Semicontinuous measurements of WSOC were made using a particle-into-liquid sampler (PILS) [*Weber et al.*, 2001; *Orsini et al.*, 2003], followed by online quantification of total organic carbon (TOC) every 6 min using a TOC analyzer (Model 810; Sievers, Boulder, CO) [*Sullivan et al.*, 2004; *Miyazaki et al.*, 2006]. Ambient aerosol was sampled at a flow rate of 16.7 L min^{-1} by the PILS, which used a steam saturator to grow the aerosol to sizes that can be collected by inertial impaction. The liquid sample (at a flow rate of 1.2 mL min^{-1}), controlled by a syringe pump, was then filtered through a 0.22-μm liquid filter (a polypropylene syringe filter, 17 mm in diameter). The carbonaceous com-

Table 1. Summary of the Laboratory Experiments for the DAX-8 Resin Using Organic Species Standards[a]

Compound Group	Compounds	MW[b] (g mol^{-1})	Concentrations (μgC L^{-1})	Penetration (%)	Definition in This Study	
					Hydrophilic	Hydrophobic
Dicarboxylic acid	Oxalic acid (C_2)	90	50, 260, 430	101, 99, 100	○	
	Succinic acid (C_4)	118	380	101	○	
	Maleic acid (C_4)	116	405	100	○	
	Fumaric acid (C_4)	116	470	0		○
	Adipic acid (C_6)	146	120	0		○
	Azelaic acid (C_9)	188	280	0		○
Carbonyls	Glyoxal	58	120	100	○	
	Methyl glyoxal	72	90	100	○	
Amines	Ethanolamine	61	160	100	○	
Saccharides	Levoglucosan	162	330	100	○	
	Sucrose	342	80, 290	100, 100	○	
Phenols	Catechol	110	220	0		○
	Syringaldehyde	182	290	0		○
Aromatic acids	Phthalic acid	166	200	0		○
Cyclic acids	Pinic acid	186	110	0		○
	cis-Pinonic acid	184	320	0		○
Humic substance	Suwannee River fulvic acid	–	70, 250, 520	0, 0, 0		○

[a]The classification as hydrophilic or hydrophobic for each compound is indicated by circles on the basis of their penetration efficiency through the DAX-8 resin.
[b]MW, molecular weight.

pounds in the liquid sample were quantified online with a TOC analyzer that operated at a continuous flow rate of 0.35 mL min^{-1}. In the present study, the term total WSOC (TWSOC) is operationally defined as particles sampled by the PILS and detected by the TOC analyzer after passing through the liquid filter (i.e., organic compounds dissolved in water or particles with a diameter <0.22 μm). A detection limit of the TWSOC concentration in this measurement system is estimated to be 0.1 μgC m^{-3}.

[8] To isolate the TWSOC components into hydrophilic and hydrophobic fractions, we used a macroporous nonionic resin (DAX-8) with TOC detection [*Duarte and Duarte*, 2005; *Sullivan and Weber*, 2006]. Many previous studies have used the XAD-8 resin to isolate hydrophobic fractions of organic compounds, mainly humic substances, from natural waters. However, because the XAD-8 resin is no longer commercially available, a substitute resin, DAX-8, was utilized in the present study. The technical specifications (e.g., pore size and surface area) and adsorption characteristics of these two resins have been shown to differ very little [e.g., *Peuravuori et al.*, 2001]. The mechanism for the organic solutes adsorption onto these resins is related to the molecular size of the solute in a water sample and to certain hydrophobic/hydrophilic interactions between the organic solutes and the nonionic sorbing solid under preadjusted conditions (e.g., pH 2).

[9] The instrumental setting of the PILS-TOC system for sequential online measurements is basically the same as that coupled with a XAD-8 resin column reported by *Sullivan and Weber* [2006]. In our measurement system, the volume of DAX-8 resin in the column was 5 mL. The WSOC solution sampled by the PILS was adjusted to pH 2 with hydrochloric acid (HCl), before continuously being pumped onto the DAX-8 resin at a flow rate of 1.3 mL min^{-1}. The DAX resin then retains hydrophobic compounds in the sample solution. In this study, we defined hydrophilic WSOC ($WSOC_{HPI}$) as organic compounds that passed through the DAX-8 column and were detected by the TOC analyzer every 6 min. A 10-port actuated valve in the liquid sample line was periodically switched to measure TWSOC for 2.5 hours, followed by $WSOC_{HPI}$ measurements for 3.5 hours. During the TWSOC measurements, the $WSOC_{HPO}$ retained by the DAX-8 column was automatically washed out with 0.1 M sodium hydroxide (NaOH) for 1.5 hours, followed by 0.1 M HCl for 0.5 hour, both at flow rates of 1.3 mL min^{-1}. By interpolating the measured time series of the TWSOC and $WSOC_{HPI}$, the difference between TWSOC and $WSOC_{HPI}$ was then defined as hydrophobic WSOC ($WSOC_{HPO}$). Because the $WSOC_{HPO}$ was determined from the TWSOC and $WSOC_{HPI}$, there may be some uncertainty in the determination of the mass concentration of the $WSOC_{HPO}$ because of the interpolation.

[10] To reduce positive artifacts (i.e., adsorption of VOCs) for the TWSOC measurements, a parallel plate diffusion denuder [*Eatough et al.*, 1993] was placed upstream of the PILS. The blank levels of WSOC were measured automatically for 30 min every 3 hours, by passing the sample air through a Teflon filter upstream of the PILS. Consequently, data for the blank level were obtained in almost every measurement mode of TWSOC and $WSOC_{HPI}$. The uncertainties in the TWSOC and $WSOC_{HPI}$ measurements in this study were estimated to be ±9% and ±12%, respectively.

2.2. Laboratory Calibration Using the DAX-8 Resin

[11] To characterize the DAX-8 resin under the current operating conditions, authentic standards of organic compounds relevant to atmospheric aerosols were tested in the laboratory, to characterize the penetration efficiency of these compounds through the column. The standards of water-soluble organic species were dissolved in purified water and were adjusted to pH 2 using HCl. They were then pumped onto the column at the same flow rate as that for the ambient sampling, followed by detection by the TOC analyzer. The organic compounds selected for this test and their penetration results are summarized in Table 1.

[12] The calibration in the laboratory showed that aliphatic dicarboxylic acids and carbonyls (<4 carbons), saccharides, and amines were classified as hydrophilic WSOC ($WSOC_{HPI}$). The hydrophobic WSOC ($WSOC_{HPO}$) included aliphatic dicarboxylic acids and carbonyls (>3–4 carbons), aromatic acids, phenols, organic nitrates, cyclic acids, and Suwannee River fulvic acids. These results confirm that

$WSOC_{HPI}$ is representative of WSOC compounds that are highly water soluble, and of low molecular weights, while $WSOC_{HPO}$ is generally represented by compounds with longer carbon chain length and/or with higher molecular weights. For C_4 dicarboxylic acids, maleic and fumaric acids are cis-trans isomers and have almost identical molecular weights. However, the water solubility of maleic acid is about 100 times higher than that of fumaric acid. This difference in chemical property can explain the result that fumaric acid was retained on the DAX resin whereas maleic acid passed through it (Table 1). It is noted that aromatic-containing compounds are included in $WSOC_{HPO}$, even if their molecular weights are low (e.g., catechol). We should also note that the aerosol WSOC and Suwannee River fulvic acid may have dissimilarities in terms of their chemical properties [e.g., *Dinar et al.*, 2006; *Graber and Rudich*, 2006; *Duarte et al.*, 2007], and the present results should be viewed as a guide to the types of fractionated WSOC compounds in ambient aerosol.

[13] The calibration results obtained here were basically the same as those reported using the XAD-8 resin [*Sullivan and Weber*, 2006]. Some compounds in the $WSOC_{HPI}$ components can be further fractionated, according to whether they can be desorbed from the DAX-8 resin with a basic solution (e.g., NaOH) [*Duarte and Duarte*, 2005]. In this study, however, we did not conduct any such "recovery" test for the DAX-8 resin.

[14] These experiments were made by changing the concentrations of organic standard solutions for several species. The resulting penetration efficiencies for the column were not affected by the amount of organic species dissolved in water, within a range of 50 to 520 μgC L^{-1}. This concentration range is similar to that observed for ambient air sampled by the PILS for at least the standards examined in this study. Because of the limited number of organic species examined, there are uncertainties in the penetration of various dissolved organic species from ambient aerosols which were not tested or remain unidentified.

2.3. Other Measurements

[15] Mass concentrations of OC and EC were measured using a semicontinuous OC/EC analyzer (Sunset Laboratory, Inc., Tigard, OR, USA) [*Birch and Cary*, 1996]. The instrument collected ambient aerosol particles on a quartz-fiber filter for 45 min at a flow rate of 8 L min^{-1} and then analyzed them by the thermal-optical-transmittance (TOT) method for 15 min. To adjust the flow rate to the cyclone (16.7 L min^{-1}), an additional pump was used for collecting ambient aerosol samples. The temperature protocol in this study was basically the same as that used in our previous studies [*Miyazaki et al.*, 2007], except that the highest temperature was 740°C instead of 870°C in the He mode. *Takegawa et al.* [2009a] found a nonnegligible negative offset of the OC data (~4.6 μg m^{-3}) by comparing organic matter (OM) measured by an Aerodyne aerosol mass spectrometer (AMS; Aerodyne Research, Inc., Billerica, MA) with the Sunset OC data used in this study. This offset is likely caused by the simple subtraction of instrumental blanks (e.g., VOC artifacts) in the Sunset OC data [*Offenberg et al.*, 2007; *Takegawa et al.*, 2009a], which may yield some uncertainties in the present analysis. Using the measured mass concentrations of OC and TWSOC, water-insoluble OC (WIOC) is defined as WIOC = OC − TWSOC.

[16] The mass loadings of sulfate in submicron aerosols were measured using an Aerodyne AMS, with a time resolution of 10 min [*Jayne et al.*, 2000; *Takegawa et al.*, 2009a]. The diameters measured by the AMS represent dry diameters because the sample air was dried before introduction into the AMS [*Takegawa et al.*, 2009a]. The AMS measures the vacuum aerodynamic diameter [*DeCarlo et al.*, 2004], the cutoff of which is roughly similar to the PM_1 (1 μm diameter cutoff size) [*Jayne et al.*, 2000].

[17] For the TWSOC, $WSOC_{HPI}$, and OC/EC measurements, $PM_{2.5}$ (2.5 μm diameter cutoff size) cyclones (URG-2000-30EHB; URG Corp., Chapel Hill, NC) were used during the first half (6–17 July) of the measurement period, and PM_1 cyclones (URG-2000-30EHB; URG Corp.) were used during the second half (17–31 July). The result showed that the median TWSOC mass concentration in the $PM_{2.5}$ mode (4.1 μgC m^{-3}) was similar to that in the PM_1 mode (4.0 μgC m^{-3}). Similarly, the median OC concentrations in the $PM_{2.5}$ (6.3 μgC m^{-3}) and PM_1 (6.1 μgC m^{-3}) modes were similar. Moreover, an average ratio of organic matter (OM) measured by the AMS to OC during the second half of the period (OM/OC = 1.88) [*Takegawa et al.*, 2009a] was similar to that found during the first half (OM/OC = 1.79), even though the size cut of OM was the same throughout the period. These results indicate that the observed TWSOC and OC were dominantly in the PM_1 mode during the measurement period. Consequently, all the TWSOC and OC data are treated as fine-mode data in the present study.

[18] Nitrogen oxides (NO_x = NO + NO_2) and total reactive nitrogen (NO_y) were measured at a 1-min time resolution using a chemiluminescence detector (TECO42S and TECO42CTL) combined with a photolytic converter (DRI blue-ray converter) and a gold tube converter [*Kondo et al.*, 2008]. SO_2 was measured using a pulsed-UV fluorescence technique with an integration time of 1 min (model 43C, Thermo Electron Corporation [TECO], Waltham, MA) [*Miyakawa et al.*, 2007]. Carbon monoxide (CO) was measured using a nondispersive infrared absorption technique with an integration time of 1 min (model48, TECO). The performance of the CO instrument has been described by *Takegawa et al.* [2009b].

[19] For nonmethane hydrocarbon (NMHC) and halocarbon measurements, ambient air was collected in evacuated 2-L stainless-steel canisters, equipped with a bellows valve. The collected samples were analyzed and quantified using a multidimension gas chromatograph-flame ionization detector (GC-FID) electron capture dissociation-mass spectrometry (ECD-MS) system. Detailed descriptions of the analysis and data quality have been presented previously [*Colman et al.*, 2001]. On average, samplings were made 5–6 times a day, and 106 samples in total were taken at the BG site. The actual integration time was 5–10 s for each sample.

[20] Local meteorological parameters were measured every 10 min by weather transmitter (WXT-510, Vaisala, Finland) at the rooftop of the observatory. During the study period, the average ambient temperature and relative humidity (RH) were 28.9 ± 3.2°C and 78.1 ± 13.6%, respectively. The planetary boundary layer height (PBLH) was derived from a two-wavelength polarization lidar measurement [*Sugimoto et*

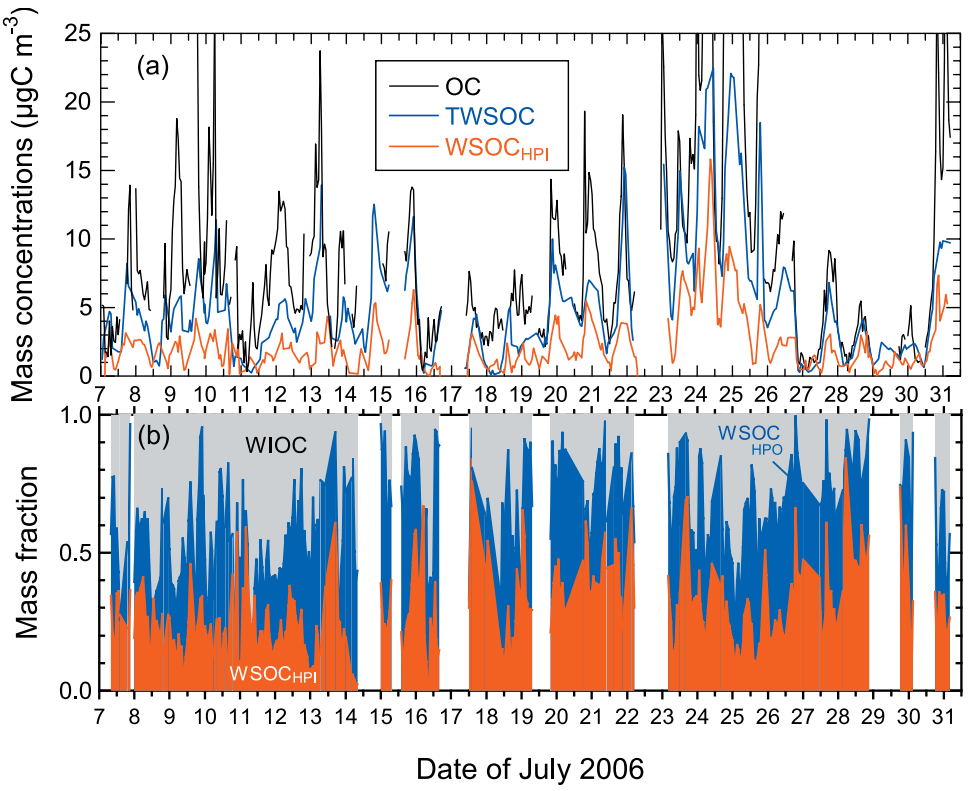

Figure 2. Time series plots of (a) the mass concentrations of OC, TWSOC, and $WSOC_{HPI}$, and (b) the mass fractions of WIOC, $WSOC_{HPO}$, and $WSOC_{HPI}$ observed between 7 and 31 July 2006.

al., 2002], conducted in Guanzhou (GZ) city. Although the sampling site at BG was about 50 km from GZ where urban heat island effects may increase the PBLH, the PBLH observed at the GZ site was assumed to be similar to that at the BG site.

2.4. Local Meteorology

[21] The measurement campaign took place during the summer season dominated by the southeast monsoon in East Asia. A high-pressure ridge over the northwestern Pacific resulted in prevailing air flow from the southerly to southeasterly direction. Figure 1 also includes the observed frequencies of the local wind direction, with wind speed greater than 1 m s^{-1} at the sampling site. In fact, the predominant local wind direction during the study period was from the southeast and southwest. Consequently, the air sampled at the BG during the measurement period was frequently influenced by emissions from major urban areas such as Guangzhou. The approximate timescale of air-mass transport from urban Guangzhou to the sampling site was estimated to be about 3–7 hours by assuming a typical wind speed of 2–4 m s^{-1}. The air sampled at the BG site was also influenced by some local sources, such as the biomass or waste burning [*Garland et al.*, 2008]. Exclusion of the effects of these local sources is described later in this paper (section 5).

[22] The observed air masses were classified into four categories according to local wind speed and wind direction. The wind-direction sectors at the sampling site were defined as northeasterly (NE; 0–90°), southeasterly (SE; 90–180°), and southwesterly (SW; 180–270°), with wind speeds greater than 1 m s^{-1}. Air masses from the northwest were neglected because they accounted for <3% of the total. In addition to these categories, air masses with wind speeds less than 1 m s^{-1} (independent of wind direction) were defined as stagnant air (SA). In the present analysis, data for air masses influenced by heavy rainfall (<1% of total) were also excluded. As a result of the classification, NE, SE, and SW data accounted for 11, 40, and 20% of the total, respectively, while SA accounted for 25%. Two-day backward trajectories were also calculated for the NE, SE, and SW air masses using the National Oceanic and Atmospheric Administration (NOAA) HYSPLIT model. The trajectories showed that their wind directions were almost consistent with the NE, SE, and SW air masses determined by the observed local wind directions (data not shown).

3. Temporal Variations

[23] Figure 2a shows time series of the mass concentrations of OC, TWSOC, and $WSOC_{HPI}$ throughout the study period. Temporal trends of the TWSOC mass concentrations were highly variable during the period. The mass concentrations of TWSOC ranged from levels below the detection limit to a maximum as high as 22 μgC m^{-3}. The median mass concentrations of OC, TWSOC, and $WSOC_{HPI}$ were 5.4, 4.1, and 1.7 μgC m^{-3}, respectively. The mass contributions of $WSOC_{HPI}$, $WSOC_{HPO}$, and WIOC to the OC concentrations are also shown in Figure 2b. On average, TWSOC accounted for 60 ± 17% of OC at the site during the study period. The mass concentration of $WSOC_{HPO}$ accounted for 60 ± 18% of TWSOC, more than that of $WSOC_{HPI}$ (40 ± 18%).

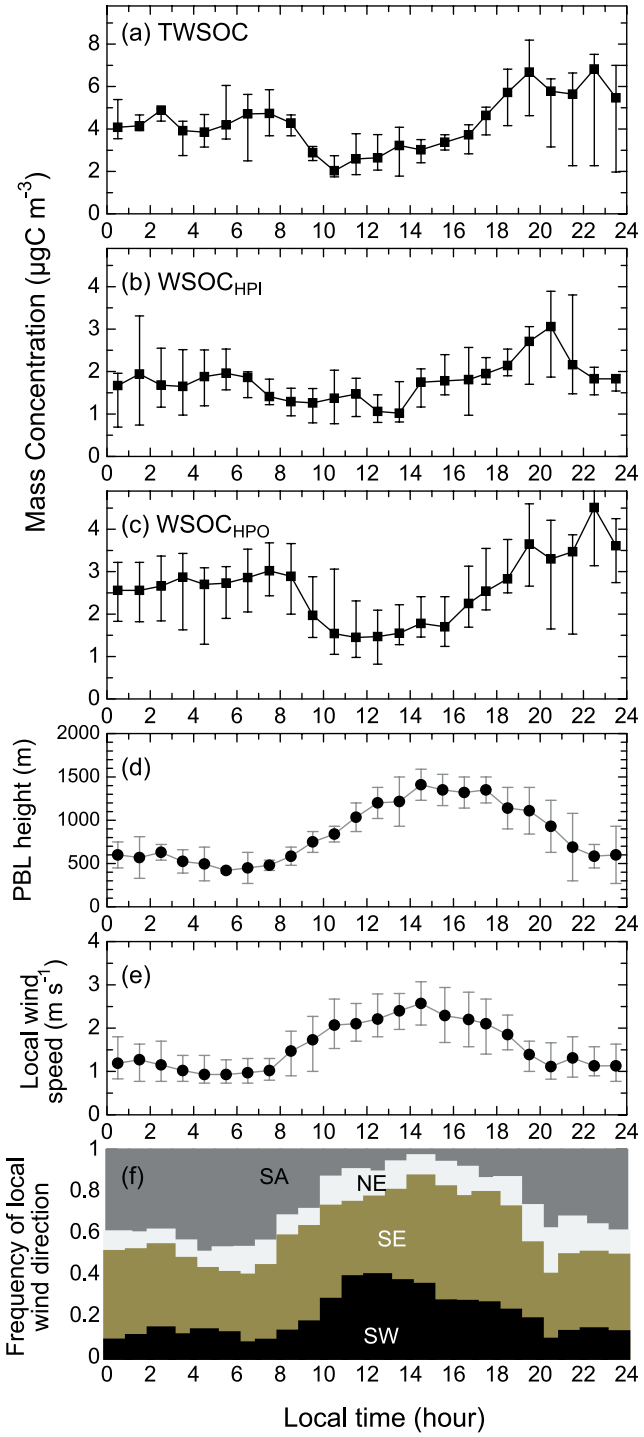

Figure 3. Diurnal variations in (a) TWSOC, (b) $WSOC_{HPI}$, (c) $WSOC_{HPO}$, (d) PBL height, (e) local wind speed, and (f) the observed frequency of local wind direction. Values shown are medians for 1-hour bins, and the bars for each value represent 67th-percentile values. Note that the PBL height was derived by lidar observations in the urban Guanzhou, located ~50 km southwest of the aerosol sampling site. SW, SE, and NE indicate southwesterly, southeasterly, and northeasterly, respectively, while SA indicates stagnated air.

[24] Extremely low levels of these species, below the instrument detection limits, were observed on days of heavy rain, on 11, 16, and 26 July. Significantly high concentrations were observed during a heavy pollution episode from 23 to 25 July, likely because of the intense local biomass burning of farming plant waste [*Garland et al.*, 2008]. Within these plumes, the mixing ratios of methyl chloride (CH_3Cl), typically used as a tracer of biomass burning, reached the maximum of 5,160 pptv. Moreover, a tight, positive correlation between CO and CH_3Cl (r^2 = 0.72) was obtained for these plumes. The slope of the regression line (dCH_3Cl/dCO) was 0.49 (pptv/ppbv), similar to the emission ratios of 0.50 – 0.57 (pptv/ppbv) from biomass burning [*Rudolph et al.*, 1995; *Andreae et al.*, 1996; *Blake et al.*, 1996; *Miyazaki et al.*, 2003]. In these plumes, the mass concentrations of OC, TWSOC, and $WSOC_{HPI}$ showed their maximum values of 80, 22, and 16 μgC m^{-3}, respectively. The average concentrations in these BB plumes were 31.9 ± 17.9μgC m^{-3} (OC), 20.2 ± 4.7 μgC m^{-3} (TWSOC), and 7.7 ± 3.0 μgC m^{-3} ($WSOC_{HPI}$). The average TWSOC/OC ratio was 63 ± 23%, which is within the range of the WSOC/OC ratios for BB plumes (45–75%) reported in previous studies [e.g., *Mayol-Bracero et al.*, 2002].

[25] Figures 3a–3c show average diurnal variations of TWSOC, $WSOC_{HPI}$, and $WSOC_{HPO}$. Figures 3a–3c present averages over the sampling period of 22 days. The mass concentrations of TWSOC, $WSOC_{HPI}$, and $WSOC_{HPO}$ showed distinct diurnal patterns, with minima occurring around noon (10:00–12:00 LT) and maxima occurring during the late afternoon and evening (16:00–23:00 LT). Figures 3d–3f show diurnal variations of PBL height, local wind speed, and the observed frequency of the local wind direction. The average height of the PBL top started to increase at around 08:00 LT, indicating the onset of convection within the PBL. The PBL height reached a maximum of around 1,400 m at 14:00–18:00 LT. The local wind speed increased in association with the increase of the PBL height, suggesting that vertical mixing in the boundary layer was more active during the daytime. Dilution in the rising PBL can affect the loss processes for TWSOC at the surface site during the daytime. With regard to the local wind direction, the relative contribution of the SE air was almost constant (~40%), while the contribution of the SW air showed a maximum of 40% during the daytime.

[26] It is interesting to note that TWSOC started to increase after 12:00 LT, despite the maximum of PBL height and active vertical mixing. This result suggests that photochemical processes were significant contributors to the observed mass concentrations of TWSOC. The relationship between the TWSOC mass and degree of photochemical processing is discussed below.

4. Dependence of the WSOC Fractions on Different Air Masses

4.1. Air Mass Characteristics

[27] Figure 4 shows the relationship between local wind speed and wind direction at the sampling site, color coded according to the mass concentrations of TWSOC and $WSOC_{HPI}$, and the mixing ratios of CO, NO_y, and SO_x (= SO_2 + SO_4^{2-}). CO is often used as a tracer of the

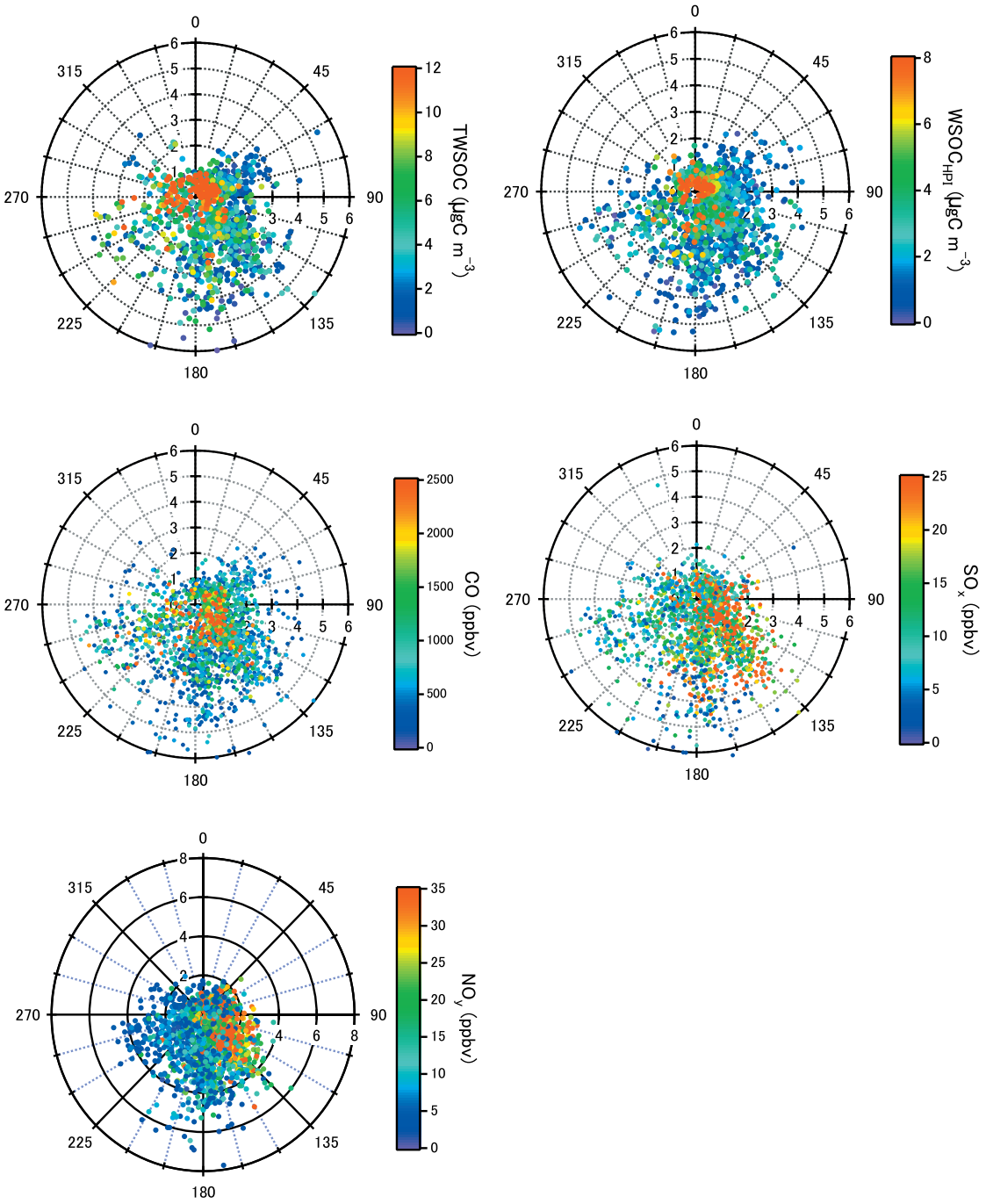

Figure 4. Relationship between local wind speed and wind direction observed at the sampling site, color coded according to the mass concentrations of TWSOC and $WSOC_{HPI}$, and the mixing ratios of CO, SO_x (= SO_2 + SO_4^{2-}), and NO_y.

primary emission of pollutants. Elevated mixing ratios of CO, NO_y, and SO_x were observed in air masses originating from the southeast direction, likely because of the strong influence of nitrogen and sulfur emissions. On the other hand, similar dependence of the observed concentrations on the wind directions was not clearly observed for TWSOC and $WSOC_{HPI}$. According to emission inventory for the PRD region [*Streets et al.*, 2003], CO, NO_x, and SO_2 are strongly emitted over the region south of the sampling site, particularly over the urban Guangzhou (GZ) and its surrounding region (Figure 1). In fact, back trajectories showed that these air masses had passed over the urban GZ region. For the emission of NO_x in the PRD region, motor vehicles (~30%) and power generation (~30%) contributed to the total emissions [*Chan and Yao*, 2008]. The emission of SO_2 in this region is likely dominated by power generation and industrial activity [*Wang et al.*, 2005].

[28] To investigate the chemical characteristics of WSOC in different air masses encountered during the study period, the frequency distributions of the observed CO, NO_x/NO_y,

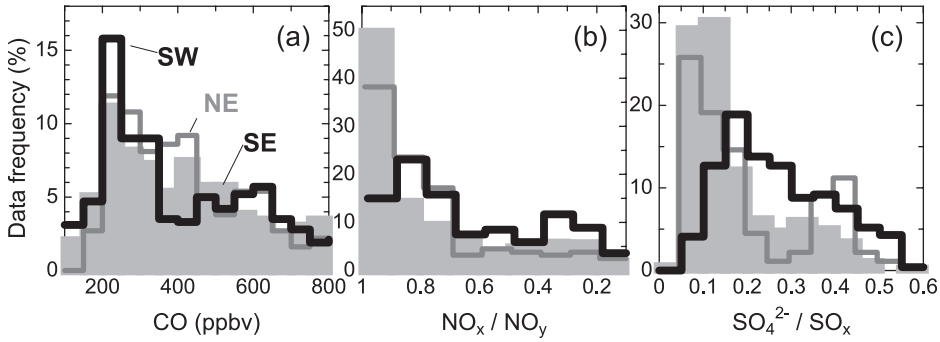

Figure 5. Frequency distributions of the observed CO, NO_x/NO_y, and SO_4^{2-}/SO_x in air masses classified by local wind direction. SW, SE, and NE indicate air-mass categories for southwesterly, southeasterly, and northeasterly, respectively. Note that the NO_x/NO_y ratios are shown from high to low values to illustrate photochemical aging running from (left) fresh to (right) aged, corresponding to aging by the SO_4^{2-}/SO_x ratios.

and SO_4^{2-}/SO_x in each air-mass category are shown in Figure 5. The NO_x/NO_y and SO_4^{2-}/SO_x ratios are used as indicators of photochemical processing. These plots clearly show differences in photochemical processing in each air mass. The frequency distributions for CO were similar for each wind-direction category, although the median CO in the SE air (457 ppbv) was the highest. For the SE air, the NO_x/NO_y ratios showed a relatively sharp peak at 0.90, while the solid lines (SW) showed a broader distribution and peaked near 0.30 and 0.80. Relatively low NO_x/NO_y ratios in the SW indicate more aged characteristics of the SW air mass. The SO_4^{2-}/SO_x ratios in the SW air (peaked near 0.20) were higher than those in the SE air (with peak at 0.10), consistent with more photochemically aged characteristics of the observed aerosols in the SW air masses compared with the SE and NE air masses.

4.2. Total and Fractionated WSOC

[29] Figure 6 illustrates the frequency distributions of the observed mass concentrations of TWSOC, $WSOC_{HPI}$, and $WSOC_{HPO}$ in each air-mass category. Median values of each component are also summarized in Table 2. The mass concentrations of TWSOC and $WSOC_{HPO}$ significantly depended on the classified air masses. The frequency distribution of the $WSOC_{HPO}$ in the SW air masses peaked at 3–4 μgC m^{-3}, with a broader distribution. The median value of $WSOC_{HPO}$ in the SW air masses (3.1 μgC m^{-3}) was substantially higher than those in the SE (2.0 μgC m^{-3}) and NE (1.6 μgC m^{-3}) air masses. The median $WSOC_{HPI}$ of 1.9 μgC m^{-3} in the SW air was also slightly higher than those in the SE and NE air masses, although the differences in mass were much larger for $WSOC_{HPO}$.

[30] TWSOC/OC ratios provide valuable clues as to the composition of and chemical processes in organic aerosols. Figure 7 shows the frequency distributions of $WSOC_{HPO}$/TWSOC and TWSOC/OC in each air mass. As expected from Figure 6, the $WSOC_{HPO}$/TWSOC ratios in the SW air were generally larger than those in the SE and NE air. The frequency distribution of the TWSOC/OC in the SW air peaked at 0.6–0.8, with a median of 0.66. This value was substantially larger than those of the SE (0.53) and NE (0.54) air. These differences in the TWSOC/OC ratios were caused by a noticeable increase in the relative contribution of the $WSOC_{HPO}$ to OC in the SW air. On average, the $WSOC_{HPO}$ fraction alone made up 44% of the OC in the SW air. These results suggest that the $WSOC_{HPO}$ mass was an important factor that controlled the water-soluble fractions of OC at the site.

[31] The frequency distributions showed that the mass of $WSOC_{HPO}$ dominated the TWSOC in more photochemically processed air masses. This suggests that the amount of $WSOC_{HPO}$ might be affected by photochemical processing.

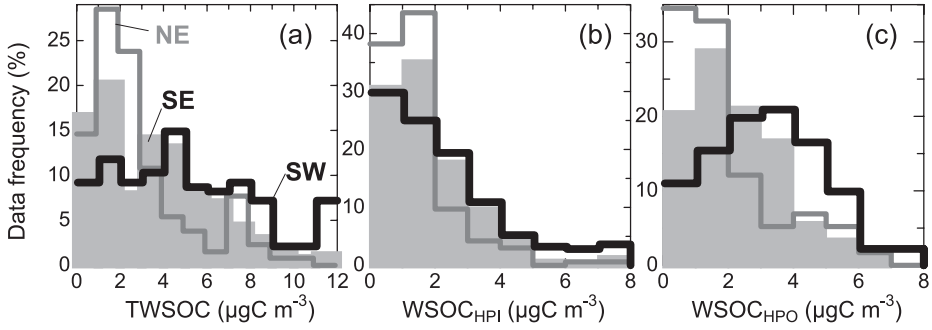

Figure 6. Same as Figure 5 but for the mass concentrations of (a)TWSOC, (b)$WSOC_{HPI}$, and (c)$WSOC_{HPO}$.

Table 2. Median Values of Each Parameter in the Three Air-Mass Categories, Defined by the Local Wind Direction[a]

Regime	TWSOC (μgC m^{-3})	$WSOC_{HPI}$ (μgC m^{-3})	$WSOC_{HPO}$ (μgC m^{-3})	WIOC (μgC m^{-3})	OC (μgC m^{-3})	TWSOC/OC	CO (ppbv)
Southwesterly (SW) ND = 91	4.9 (3.6–6.7)	1.9 (1.3–2.8)	3.1 (2.1–3.9)	1.9 (1.1–2.5)	7.1 (4.7–9.2)	0.66 (0.57–0.72)	457 (261–741)
Southeasterly (SE) ND = 181	3.9 (2.9–4.8)	1.6 (1.2–2.3)	2.0 (1.4–2.7)	2.1 (1.2–2.4)	6.0 (4.1–7.2)	0.53 (0.45–0.67)	477 (290–826)
Northeasterly (NE) ND = 53	3.1 (2.4–4.0)	1.5 (1.0–2.0)	1.6 (1.4–3.2)	1.4 (0.8–4.2)	4.5 (3.2–9.2)	0.54 (0.50–0.58)	432 (299–738)

[a]Numbers in parentheses are ±67th percentiles.

Figure 8 shows scatter plots between OC and EC for the SE and SW air masses color coded according to the mass concentrations of TWSOC. The SE and SW air masses are compared here because both had passed over urban regions south of the sampling site in the PRD region (Figure 1) according to the backward trajectories. The linear regression slope of the OC/EC for the SW air was 2.65, much larger than that in the SE air (1.61). These values are also larger than the OC/EC ratios of primary emissions (1.3–1.4) reported for GZ and other urban areas in China [*Cao et al.*, 2003; *Andreae et al.*, 2008]. Additionally, the TWSOC mass concentrations tended to be greater with increasing OC/EC slopes as seen from Figure 8. These results support the photochemically aged characteristics of the SW air and are indicative of the secondary production of OC.

[32] It is noted that on a mass basis, a considerable fraction of biomass-burning (BB) aerosols has been shown to consist of hydrophobic organic compounds, with high molecular weights, or HULIS [*Mayol-Bracero et al.*, 2002; *Feczko et al.*, 2007; *Asa-Awuku et al.*, 2008]. It is difficult to quantitatively determine the contribution of BB to the observed WSOC from our measurement data alone. However, the weak correlation between WSOC and CH_3Cl (r^2 = 0.29; data not shown) as a tracer of BB emissions in the SW air masses suggests that BB sources contributed to the observed $WSOC_{HPO}$ to some degree during the study period. While the frequency distributions of the $WSOC_{HPO}$ mass concentrations were significantly different in each air mass, the average mixing ratios of CH_3Cl were similar in all air-mass categories (841 ± 361, 840 ± 316, and 827 ± 140 pptv in the NE, SE, and SW air masses, respectively). Moreover, several previous studies have indicated that primary, urban emissions of WSOC are negligible [*Miyazaki et al.*, 2006; *Huang et al.*, 2006; *Weber et al.*, 2007]. Consequently, the observed $WSOC_{HPO}$ in the SW air masses was primarily photochemically processed rather than significantly influenced by primary emissions of biomass burning or urban sources.

5. Chemical Evolution of Fractionated OC

[33] To investigate the chemical evolution of fractionated OC, relationships between OC mass fractions and photochemical age are examined here. In the following analysis, we focus on the data for the SE and SW air masses.

5.1. Photochemical Age Using the NO_x/NO_y Ratio

[34] The ratio of NO_x to NO_y is used as a photochemical age to quantify the atmospheric processing of fractionated OC [*Kleinman et al.*, 2007, 2008]. NO_x is emitted primarily as NO, followed by the formation of a steady state mixture of NO and NO_2, by rapid reaction with O_3. Subsequent oxidation reaction products include HNO_3, peroxyacetyl nitrate (PAN), and alkyl nitrates. In the daytime, NO_x (primarily NO_2) is mainly oxidized to HNO_3 by reaction with OH, leading to a decreased NO_x/NO_y ratio. The present analysis defines photochemical age as $-\log(NO_x/NO_y)$ which follows the method of *Kleinman et al.* [2008], where

$$-2.303\log\left(NO_x/NO_y\right) = -\ln\left(NO_x/NO_y\right) = -k[OH]t \quad (1)$$

where k is the rate constant for NO_2 + OH, [OH] is a time-averaged OH concentration, and t is the time-integrated exposure of an air mass to OH. A photochemical age has a value of 0 for fresh emissions ($NO_y = NO_x$) and a value of 1 when NO_x/NO_y ratio of 0.1 (that is, 90% of NO_x has been oxidized).

[35] Previous studies have pointed out ambiguities and biases in determining the photochemical age of air samples that are influenced by mixtures of emission sources [*Kleinman et al.*, 2003; *Parrish et al.*, 2007]. There might not be a single

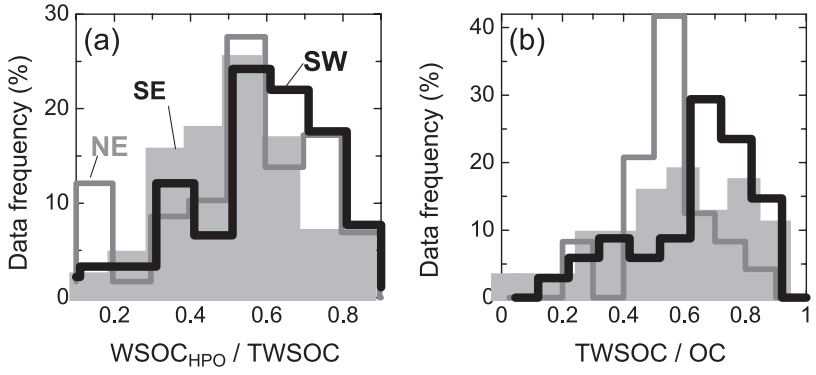

Figure 7. Same as Figure 5 but for (a)$WSOC_{HPO}$/TWSOC, and (b)TWSOC/OC.

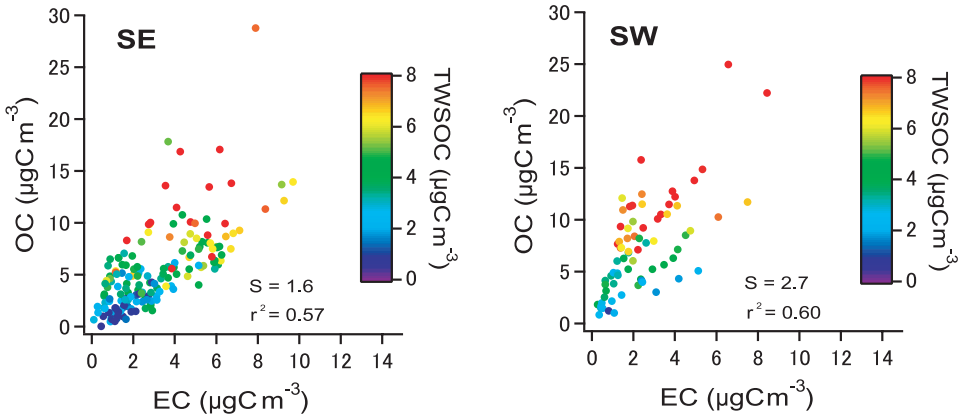

Figure 8. Scatter plots of the OC and EC mass concentrations for the (left) SE and (right) SW air masses, color coded according to the mass concentrations of TWSOC. S indicates the slope of the regression line.

well-defined atmospheric residence time because of the fact that emission sources are spatially distributed. To exclude air masses significantly influenced by local emissions, data with CO > 1,500 ppbv are not included in the following analysis. For these excluded data, the NO_x mixing ratios were significantly high (>15 ppbv), which may not be associated with the processing of aerosols considered here. After excluding the effects of local sources, the OC/EC ratios both in the SE and SW air masses tend to increase with the decrease in the NO_x/NO_y ratios (data not shown), indicative of the secondary production of OC with photochemical aging. These results indicate that although it is rather qualitative, the NO_x/NO_y ratio without significant effects of local emissions can be useful for ordering observed air masses, according to their atmospheric exposure. This means that a general increase in photochemical age is not necessarily caused by the distance from the source by direct transport. It is also noted that although most of the samples analyzed here were obtained during the daytime, part of the samples may have spent their atmospheric residence during the night where $NO_2 + O_3$ is considered to be the major reaction pathway for oxidation of NO_x.

[36] When considering photochemical changes in the organic mass, the effect of dilution should be taken into account by normalizing concentrations to a conservative tracer on the timescale of interest. To calculate the change in the mass fractions of $WSOC_{HPI}$, $WSOC_{HPO}$, and WIOC as a function of photochemical age, the OC compositions were normalized by CO, used as a conservative tracer. Although CO is slowly oxidized in the atmosphere, it can be regarded as inert over the timescale considered here (hours to a day). The background CO value of 160 ppbv was in approximately the lowest fifth percentile of the CO mixing ratio observed during the study period. In the following section, Δ refers to an enhancement of a concentration over the background value.

5.2. Fractionated OC as a Function of Photochemical Age

[37] Figure 9 shows the median OC composition as a function of photochemical age in all the air masses for four bins, according to the $-\log(NO_x/NO_y)$. A timescale can be assigned to the photochemical age when OH concentrations are given. A photochemical age of 0.8 corresponds to approximately 9 hours for average OH concentrations of about 7×10^6 molec cm^{-3} observed at the sampling site (Lu et al., manuscript in preparation).

[38] At the photochemical age of 0.0–0.2, TWSOC accounted for 45% of OC, the mass fraction of which was similar to that of WIOC. At this early stage, the mass fractions of $WSOC_{HPI}$ and $WSOC_{HPO}$ were similar. The amounts of $WSOC_{HPI}$ and $WSOC_{HPO}$ increased with atmospheric aging, leading to the predominant fraction of TWSOC (~74%) at a photochemical age of 0.6–0.8. The increase of TWSOC ($d(\Delta TWSOC/\Delta CO) \sim 0.032$ $\mu gC\ m^{-3}\ ppbv^{-1}$) is larger than that observed in urban plumes in the eastern United States after ~9 hours of processing (~0.013 $\mu gC\ m^{-3}\ ppbv^{-1}$) [*de Gouw et al.*, 2008]. The most pronounced result was that the increasing mass of $WSOC_{HPO}$ ($d(\Delta WSOC_{HPO}/\Delta CO) \sim 0.022$ $\mu gC\ m^{-3}\ ppbv^{-1}$) was substantially larger than that of $WSOC_{HPI}$ ($d(\Delta WSOC_{HPI}/\Delta CO) \sim 0.009$ $\mu gC\ m^{-3}\ ppbv^{-1}$) from a photochemical age of 0.0–0.2 to 0.6–0.8. For the photochemical age greater than 0.6, the $WSOC_{HPO}$ mass increased

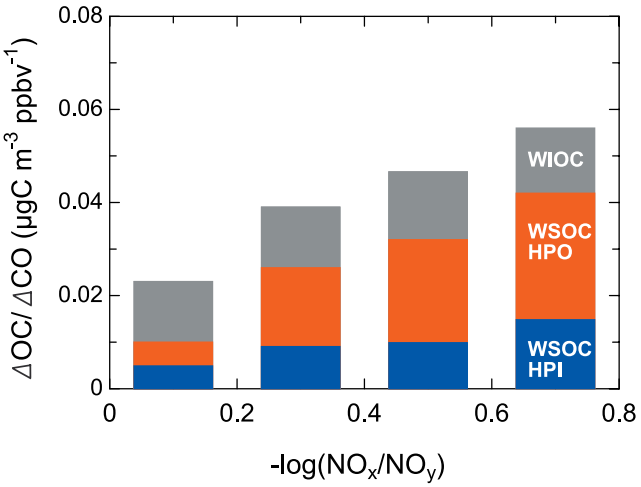

Figure 9. Fractionated ambient organic carbon aerosols as a function of the photochemical age ($-\log(NO_x/NO_y)$). Each organic mass is normalized by CO.

by a factor of 5 compared to ages less than 0.2, whereas the $WSOC_{HPI}$ only increased by a factor of 2–3. The increase in the masses of $WSOC_{HPO}$ and $WSOC_{HPI}$ with photochemical age was accompanied by addition of the SOA mass. Moreover, the total increase in the mass of TWSOC was accompanied by a noticeable increase in the relative contribution of $WSOC_{HPO}$. The results suggest that the photochemical processes produce significant levels of hydrophobic compounds that add substantially to the organic aerosol mass in the fine particles within the timescales considered here.

[39] It is also interesting to note that the normalized mass of WIOC did not exhibit noticeable changes with air-mass aging. It has been suggested that WSOC also includes aged primary components of OC as well as SOA particularly over regions remote from primary sources [*Fuzzi et al.*, 2006]. However, the less pronounced change in the WIOC mass with air-mass aging suggests that this transformation was not a dominant process for the increase in the mass of WSOC during the study period. In addition, the normalized TWSOC at a photochemical age of 0.6–0.8 far exceeded that of 0.0–0.2, whereas the amount of the WIOC showed little variation with air-mass aging within the timescale considered here. These results also support that most of the observed WSOC cannot be primary OC. *Favez et al.* [2008] indicated that WIOC can be formed as a result of SOA formation in semiarid urban atmosphere, where RH is much lower (<45%) than that at the BG site (with the average RH of 78 ± 14%). This formation also seems unlikely because of the insignificant change in the WIOC mass with air-mass aging. Given that the negative offset of the OC data is ~4.6 $\mu g\ m^{-3}$, as mentioned in section 2.3, the correction of the OC data would lead to an increase of ~55% in the average $\Delta OC/\Delta CO$. Nevertheless, this uncertainty is not responsible for the increase in $WSOC_{HPI}$ and $WSOC_{HPO}$, and it may not significantly affect the relative changes in WIOC with air-mass aging in this study.

[40] From thermograms of WSOC obtained at urban sites in China, previous studies inferred that 40–50% of the WSOC was refractory [*Yu et al.*, 2004; *Yang et al.*, 2005], most of which was related to $WSOC_{HPO}$ in this study. In the Chinese outflow observed at Gosan, Korea, highly refractory compound groups were found to be the largest contributor to the WSOC, accounting for ~80% of TWSOC by mass [*Miyazaki et al.*, 2007]. The present results differ from those reported for urban Atlanta [*Sullivan and Weber*, 2006], where the average fraction of $WSOC_{HPI}$ to TWSOC (~60%) dominated throughout the summer period. One explanation of this difference may be because of the degree of air-mass aging: air masses analyzed in Atlanta were sampled in an urban area, while air masses presented here were obtained at a rural site that had likely undergone more photochemical aging leading to $WSOC_{HPO}$-dominated air masses. In summary, the present result indicates that photochemical formation of $WSOC_{HPO}$ was a significant contributor to TWSOC.

[41] There are several possibilities for the additional mass of $WSOC_{HPO}$. Increases in the SOA yields from acid-catalyzed reactions have been proposed in previous studies [*Jang and Kamens*, 2001; *Jang et al.*, 2002]. However, these reactions seem unlikely in this study because the observed aerosols at the BG site were nearly neutralized or basic (data not shown). This is consistent with previous studies that have not found any evidence that SOA yields increase with acidity under ambient atmospheric conditions [e.g., *Peltier et al.*, 2007]. It is possible that oxidation products of VOCs that are evaporated from primary organic aerosols (POA) during the rapid dilution generate OA after emission within a timescale of a few hours [*Robinson et al.*, 2007]. Another possibility is aerosol phase polymerization reactions that yield nonvolatile products [*Kalberer et al.*, 2004]. Such a process would be consistent with a continued growth of the $WSOC_{HPO}$ mass, which is likely represented by compounds with relatively larger carbon numbers, as suggested by the laboratory calibration (section 2.2) and also with the apparent lack of an evaporated loss of the TWSOC mass. SOA formation through in-cloud processing is also a possible formation pathway [*Gelencsér et al.*, 2003]. In fact, cloud events are frequent in the PRD region and in-cloud processing has been found to be a dominant formation pathway for sulfate [e.g., *Huang et al.*, 2006]. The present findings provide a much better understanding of the formation process of organic aerosols in the real atmosphere and provide useful guidance regarding speciation of TWSOC at a molecular level.

6. Conclusions

[42] We made semicontinuous measurements of total and chemically isolated water-soluble organic carbon (WSOC) in fine aerosols at a rural site in the Pearl River Delta (PRD) region of China in July 2006. Online measurements were made using a particle-into-liquid sampler (PILS) with the DAX-8 resin. Under our operating condition, organic compounds that penetrated through the DAX-8 column were defined as hydrophilic WSOC ($WSOC_{HPI}$), while those retained by the column were defined as hydrophobic WSOC ($WSOC_{HPO}$). Laboratory calibration using organic standards showed that the $WSOC_{HPI}$ included low-molecular aliphatic dicarboxylic acids and carbonyls with carbon numbers less than four, saccharides, and amines. The $WSOC_{HPO}$ included aliphatic dicarboxylic acids and carbonyls with carbon numbers larger than 3–4, aromatic acids, phenols, organic nitrates, cyclic acids, and fulvic acids, which have relatively longer carbon chain lengths than $WSOC_{HPI}$.

[43] On average, total WSOC (TWSOC) accounted for 60% of OC at the sampling site during the study period, of which $WSOC_{HPO}$ was found to account for 60% of TWSOC. The mass fractions of TWSOC depended on the air masses classified according to the local wind directions. The $WSOC_{HPO}$ mass dominated the total WSOC composition in more photochemically processed air masses.

[44] The mass of both $WSOC_{HPI}$ and $WSOC_{HPO}$ increased with photochemical aging, determined by the observed NO_x/NO_y ratio. In particular, the average mass of $WSOC_{HPO}$ was found to increase by a factor of 5 within a timescale of about 10 hours, substantially larger than that of $WSOC_{HPI}$ (a factor of 2–3). The total increase in the mass of TWSOC with photochemical aging was accompanied by a noticeable increase in the relative contribution of the $WSOC_{HPO}$. The combined results of the field measurements and laboratory calibrations suggest that the photochemical processes produce significant levels of hydrophobic organic compounds with generally larger carbon numbers that add

substantially to the organic aerosol mass in the fine particles in this region.

[45] By contrast, the WIOC mass did not exhibit significant changes with photochemical aging, suggesting that the chemical transformation from WIOC to WSOC in aerosols was not a dominant process for the production of WSOC in the present study. These findings provide an improved understanding on the formation process of organic aerosols in the real atmosphere and provide useful guidance regarding speciation of WSOC at a molecular level.

[46] **Acknowledgments.** The authors thank A. Sullivan for providing valuable information on the PILS measurements. The authors gratefully acknowledge all of the other team members at the backyard garden site for their support during the field campaign. This research was supported by the Japanese Ministry of Education, Culture, Sports, Science and Technology (MEXT), and the global environment research fund of the Japanese Ministry of the Environment (B-083). This work was also supported by the National Basic Research Program (973 Program, 2002CB410801) and National High-tech R&D Program (863 Program, 2006AA06A308) of China.

References

Andreae, M. O., et al. (1996), Trace gas and aerosol emissions from savanna fires, in *Biomass Burning and Global Change*, edited by J. S. Levine, pp. 278–295, MIT Press, Cambridge, Mass.

Andreae, M. O., O. Schmid, H. Yang, D. Chand, J. Z. Yu, L.-M. Zeng, and Y.-H. Zhang (2008), Optical properties and chemical composition of the atmospheric aerosol in urban Guangzhou, China, *Atmos. Environ.*, *42*, 6335–6350.

Asa-Awuku, A., A. P. Sullivan, C. J. Hennigan, R. J. Weber, and A. Nenes (2008), Investigation of molar volume and surfactant characteristics of water-soluble organic compounds in biomass burning aerosol, *Atmos. Chem. Phys.*, *8*, 799–812.

Birch, M. E., and R. A. Cary (1996), Elemental carbon-based method for monitoring occupational exposures to particulate diesel exhaust, *Aerosol Sci. Technol.*, *25*, 221–241.

Blake, N. J., D. R. Blake, B. C. Sive, T.-Y. Chen, F. S. Rowland, J. E. Collins Jr., G. W. Sachse, and B. E. Anderson (1996), Biomass burning emissions and vertical distribution of atmospheric methyl halides and other reduced carbon gases in the South Atlantic region, *J. Geophys. Res.*, *101*, 24,151–24,164.

Cao, J. J., et al. (2003), Characteristics of carbonaceous aerosol in Pearl River Delta Region, China during 2001 winter period, *Atmos. Environ.*, *37*, 1451–1460.

Chan, C. K., and X. Yao (2008), Air pollution in mega cities in China, *Atmos. Environ.*, *42*, 1–42.

Colman, J. J., A. L. Swanson, S. Meinardi, B. C. Sive, D. R. Blake, and F. S. Rowland (2001), Description of the analysis of a wide range of volatile organic compounds in whole air samples collected during PEM-Tropics A and B, *Anal. Chem.*, *73*, 3731–4723.

DeCarlo, P., J. G. Slowik, D. R. Worsnop, P. Davidovits, and J. L. Jimenez (2004), Particle morphology and density characterization by combined mobility and aerodynamic diameter measurements. Part 1: Theory, *Aerosol Sci. Technol.*, *38*, 1185–1205.

Decesari, S., M. C. Facchini, S. Fuzzi, and E. Tagliavini (2000), Characterization of water-soluble organic compounds in atmospheric aerosol: A new approach, *J. Geophys. Res.*, *105*, 1481–1489.

de Gouw, J. A., et al. (2008), Sources of particulate matter in the northeastern United States in summer: 1. Direct emissions and secondary formation of organic matter in urban plumes, *J. Geophys. Res.*, *113*, D08301, doi:10.1029/2007JD009243.

Dinar, E., T. F. Mentel, and Y. Rudich (2006), The density of humic acids and humic like substances (HULIS) from fresh and aged wood burning and pollution aerosol particles, *Atmos. Chem. Phys.*, *6*, 5213–5224.

Duarte, R. M. B., and A. C. Duarte (2005), Application of non-ionic solid sorbents (XAD Resins) for the isolation and fractionation of water-soluble organic compounds from atmospheric aerosols, *J. Atmos. Chem.*, *51*, 79–93.

Duarte, R. M. B. O., E. B. H. Santos, C. A. Pio, and A. C. Duarte (2007), Comparison of structural features of water-soluble organic matter from atmospheric aerosols with those of aquatic humic substances, *Atmos. Environ.*, *41*, 8100–8113.

Eatough, D. J., A. Wadsworth, D. A. Eatough, J. W. Crawford, L. D. Hansen, and E. A. Lewis (1993), A multiple system, multi-channel diffusion denuder sampler for the determination of fine-particulate organic material in the atmosphere, *Atmos. Environ. Part A*, *27*, 1213–1219.

Facchini, M. C., M. Mircea, S. Fuzzi, and R. J. Charlson (1999), Cloud albedo enhancement by surface-active organic solutes in growing droplets, *Nature*, *401*, 257–259.

Facchini, M. C., S. Decesari, M. Mircea, S. Fuzzi, and G. Loglio (2000), Surface tension of atmospheric wet aerosol and cloud/fog droplets in relation to their organic carbon content and chemical composition, *Atmos. Environ.*, *34*, 4853–4857.

Favez, O., J. Sciare, H. Cachier, S. C. Alfaro, and M. M. Abdelwahab (2008), Significant formation of water-insoluble secondary organic aerosols in semiarid urban environment, *Geophys. Res. Lett.*, *35*, L15801, doi:10.1029/2008GL034446.

Feczko, T., H. Puxbaum, A. Kasper-Giebl, M. Handler, A. Limbeck, A. Gelencsér, C. Pio, S. Preunkert, and M. Legrand (2007), Determination of water and alkaline extractable atmospheric humic-like substances with the TU Vienna HULIS analyzer in samples from six background sites in Europe, *J. Geophys. Res.*, *112*, D23S10, doi:10.1029/2006JD008331.

Feng, J., M. Hu, C. K. Chan, P. S. Lau, M. Fang, L. He, and X. Tang (2006), A comparative study of the organic matter in $PM_{2.5}$ from three Chinese megacities in three different climatic zones, *Atmos. Environ.*, *40*, 3983–3994.

Fuzzi, S., et al. (2006), Critical assessment of the current state of scientific knowledge, terminology, and research needs concerning the role of organic aerosols in the atmosphere, climate, and global change, *Atmos. Chem. Phys.*, *6*, 2017–2038.

Garland, R. M., et al. (2008), Aerosol optical properties in a rural environment near the mega-city Guangzhou, China: Implications for regional air pollution and radiative forcing, *Atmos. Chem. Phys.*, *8*, 5161–5186.

Gelencsér, A., A. Hoffer, G. Kiss, E. Tombacz, R. Kurdi, and L. Bencze (2003), In-situ formation of light-absorbing organic matter in cloud water, *J. Atmos. Chem.*, *45*, 25–33.

Graber, E. R., and Y. Rudich (2006), Atmospheric HULIS: How humic-like are they? A comprehensive and critical review, *Atmos. Chem. Phys.*, *6*, 729–753.

Huang, X.-F., J. Z. Yu, L.-Y. He, and Z. Yuan (2006), Water-soluble organic carbon and oxalate in aerosols at a coastal urban site in China: Size distribution characteristics, sources, and formation mechanisms, *J. Geophys. Res.*, *111*, D22212, doi:10.1029/2006JD007408.

Jang, M., and R. M. Kamens (2001), Atmospheric secondary aerosol formation by heterogeneous reactions of aldehydes in the presence of a sulfuric acid aerosol catalyst, *Environ. Sci. Technol.*, *35*, 4758–4766.

Jang, M., N. M. Czoschke, S. Lee, and R. M. Kamens (2002), Heterogeneous atmospheric aerosol production by acid-catalyzed particle-phase reactions, *Science*, *298*, 814–817.

Jayne, J. T., D. C. Leard, X. F. Zhang, P. Davidovits, K. A. Smith, C. E. Kolb, and D. R. Worsnop (2000), Development of an aerosol mass spectrometer for size and composition analysis of submicron particles, *Aerosol Sci. Technol.*, *33*, 49–70.

Kalberer, M., et al. (2004), Identification of polymers as major components of atmospheric organic aerosols, *Science*, *303*, 1659–1662.

Kiss, G., E. Tombacz, and H. C. Hansson (2005), Surface tension effects of humic-like substances in the aqueous extract of tropospheric fine aerosol, *J. Atmos. Chem.*, *50*, 279–294.

Kleinman, L. I., et al. (2003), Photochemical age determinations in the Phoenix metropolitan area, *J. Geophys. Res.*, *108*(D3), 4096, doi:10.1029/2002JD002621.

Kleinman, L. I., et al. (2007), Aircraft observations of aerosol composition and ageing in New England and Mid-Atlantic States during the summer 2002 New England Air Quality Study field campaign, *J. Geophys. Res.*, *112*, D09310, doi:10.1029/2006JD007786.

Kleinman, L. I., et al. (2008), The time evolution of aerosol composition over the Mexico City plateau, *Atmos. Chem. Phys.*, *8*, 1559–1575.

Kondo, Y., Y. Miyazaki, N. Takegawa, T. Miyakawa, R. J. Weber, J. L. Jimenez, Q. Zhang, and D. R. Worsnop (2007), Oxygenated and water-soluble organic aerosols in Tokyo, *J. Geophys. Res.*, *112*, D01203, doi:10.1029/2006JD007056.

Kondo, Y., et al. (2008), Formation and transport of oxidized reactive nitrogen, ozone, and secondary organic aerosol in Tokyo, *J. Geophys. Res.*, *113*, D21310, doi:10.1029/2008JD010134.

Mayol-Bracero, O. L., P. Guyon, B. Graham, G. Roberts, M. O. Andreae, S. Decesari, M. C. Facchini, S. Fuzzi, and P. Artaxo (2002), Water-soluble organic compounds in biomass burning aerosols over Amazonia: 2. Apportionment of the chemical composition and importance of the polyacidic fraction, *J. Geophys. Res.*, *107*(D20), 8091, doi:10.1029/2001JD000522.

Miyakawa, T., N. Takegawa, and Y. Kondo (2007), Removal of sulfur dioxide and formation of sulfate aerosol in Tokyo, *J. Geophys. Res.*, *112*, D13209, doi:10.1029/2006JD007896.

Miyazaki, Y., et al. (2003), Synoptic-scale transport of reactive nitrogen over the western Pacific in spring, *J. Geophys. Res.*, *108*(D20), 8788, doi:10.1029/2002JD003248.

Miyazaki, Y., Y. Kondo, N. Takegawa, Y. Komazaki, M. Fukuda, K. Kawamura, M. Mochida, K. Okuzawa, and R. J. Weber (2006), Time-resolved measurements of water-soluble organic carbon in Tokyo, *J. Geophys. Res.*, *111*, D23206, doi:10.1029/2006JD007125.

Miyazaki, Y., Y. Kondo, S. Han, M. Koike, D. Kodama, Y. Komazaki, H. Tanimoto, and H. Matsueda (2007), Chemical characteristics of water-soluble organic carbon in the Asian outflow, *J. Geophys. Res.*, *112*, D22S30, doi:10.1029/2007JD009116.

Novakov, T., and J. E. Penner (1993), Large contribution of organic aerosols to cloud-condensation-nuclei concentrations, *Nature*, *365*, 823–826.

Offenberg, J. H., M. Lewandowski, E. O. Edney, T. E. Kleindienst, and M. Jaoui (2007), Investigation of a systematic offset in the measurement of organic carbon with a semicontinuous analyzer, *J. Air Waste Manage. Assoc.*, *53*, 84–91.

Orsini, D. A., Y. Ma, A. Sullivan, B. Sierau, K. Baumann, and R. J. Weber (2003), Refinements to the particle-into-liquid sampler (PILS) for ground and airborne measurements of water soluble aerosol composition, *Atmos. Environ.*, *37*, 1243–1259.

Parrish, D. D., A. Stohl, C. Forster, E. L. Atlas, D. R. Blake, P. D. Goldan, W. C. Kuster, and J. A. de Gouw (2007), Effects of mixing on evolution of hydrocarbon ratios in the troposphere, *J. Geophys. Res.*, *112*, D10S34, doi:10.1029/2006JD007583.

Peltier, R. E., A. P. Sullivan, R. J. Weber, A. G. Wollny, J. S. Holloway, C. A. Brock, J. A. de Gouw, and E. L. Atlas (2007), No evidence foracid-catalyzed secondary organic aerosol formation in power plant plumes over metropolitan Atlanta, Georgia, *Geophys. Res. Lett.*, *34*, L06801, doi:10.1029/2006GL028780.

Peuravuori, J., P. Ingman, K. Pihlaja, and R. Koivikko (2001), Comparisons of aquatic humic matter by DAX-8 and XAD-8 resins from solid-state 13C NMR spectroscopy's point of view, *Talanta*, *55*, 733–742.

Robinson, A. L., N. M. Donahue, M. K. Shrivastava, E. A. Weitkamp, A. M. Sage, A. P. Grieshop, T. E. Lane, J. R. Pierce, and S. N. Pandis (2007), Rethinking organic aerosols: Semivolatile emissions and photochemical aging, *Science*, *315*, 1259–1262.

Rudolph, J., A. Khedim, R. Koppmann, and B. Bonsang (1995), Field study of the emissions of methyl chloride and other halocarbons from biomass burning in Western Africa, *J. Atmos. Chem.*, *22*, 67–80.

Saxena, P., L. M. Hildemann, P. H. McMurry, and J. H. Seinfeld (1995), Organics alter hygroscopic behavior of atmospheric particles, *J. Geophys. Res.*, *100*, 18,755–18,770.

Streets, D. G., et al. (2003), An inventory of gaseous and primary aerosol emissions in Asia in the year 2000, *J. Geophys. Res.*, *108*(D21), 8809, doi:10.1029/2002JD003093.

Sugimoto, N., I. Matsui, A. Shimizu, I. Uno, K. Asai, T. Endoh, and T. Nakajima (2002), Observation of dust and anthropogenic aerosol plumes in the northwest Pacific with a two-wavelength polarization lidar on board the research vessel Mirai, *Geophys. Res. Lett.*, *29*(19), 1901, doi:10.1029/2002GL015112.

Sullivan, A. P., and R. J. Weber (2006), Chemical characterization of the ambient organic aerosol soluble in water: 1. Isolation of hydrophobic and hydrophilic fractions with a XAD-8 resin, *J. Geophys. Res.*, *111*, D05314, doi:10.1029/2005JD006485.

Sullivan, A. P., R. J. Weber, A. L. Clements, J. R. Turner, M. S. Bae, and J. J. Schauer (2004), A method for on-line measurement of water-soluble organic carbon in ambient aerosol particles: Results from an urban site, *Geophys. Res. Lett.*, *31*, L13105, doi:10.1029/2004GL019681.

Takegawa, N., et al. (2009a), Performance of an Aerodyne aerosol mass spectrometer (AMS) during intensive campaigns in China in the summer of 2006, *Aerosol Sci. Technol.*, *43*, 189–204.

Takegawa, N., et al. (2009b), Variability of submicron aerosol observed at a rural site in Beijing in the summer of 2006, *J. Geophys. Res.*, *114*, D00G05, doi:10.1029/2008JD010857.

Wang, X., G. Carmichael, D. Chen, Y. Tang, and T. Wang (2005), Impacts of different emission sources on air quality during March 2001 in the Pearl River Delta (PRD) region, *Atmos. Environ.*, *39*, 5227–5241.

Weber, R. J., D. Orsini, Y. Daun, Y.-N. Lee, P. J. Klotz, and F. Brechtel (2001), A particle-into-liquid collector for rapid measurement of aerosol bulk chemical composition, *Aerosol Sci. Technol.*, *35*, 718–727.

Weber, R. J., et al. (2007), A study of secondary organic aerosol formation in the anthropogenic-influenced southeastern United States, *J. Geophys. Res.*, *112*, D13302, doi:10.1029/2007JD008408.

Yang, H., et al. (2005), The chemical composition of inorganic and carbonaceous materials in $PM_{2.5}$ in Nanjing, China, *Atmos. Environ.*, *39*, 3735–3749.

Yu, J. Z., H. Yang, H. Zhang, and A. K. H. Lau (2004), Size distributions of water-soluble organic carbon in ambient aerosols and its size-resolved thermal characteristics, *Atmos. Environ.*, *38*, 1061–1071.

Zheng, M., T. S. M. Wan, M. Fang, and F. Wang (1997), Characterization of the non-volatile organic compounds in the aerosols of Hong Kong—Identification, abundance and origin, *Atmos. Environ.*, *31*, 227–237.

Zhang, Q., et al. (2009), Asian emissions in 2006 for the NASA INTEX-B mission, *Atmos. Chem. Phys. Disc.*, *9*, 4081–4139.

D. R. Blake, Department of Chemistry, University of California, Irvine, CA 92697-2025, USA.

Z. Q. Deng and M. Hu, State Key Joint Laboratory of Environmental Simulation and Pollution Control, College of Environmental Sciences and Engineering, Peking University, Beijing 100871, China.

S. Han, Y. Kondo, T. Miyakawa and N. Takegawa, Research Center for Advanced Science and Technology, University of Tokyo, 4-6-1 Komaba, Meguro-ku, Tokyo 153-8904, Japan.

K. Kita, Department of Environmental Science, Ibaraki University, 20101 Bunkyo, Mito, Ibaraki 310-8512, Japan.

Y. Miyazaki, Institute of Low Temperature Science, Hokkaido University, N19, W8, Kita-ku, Sapporo 060-0819, Japan. (yuzom@lowtem.hokudai.ac.jp)

M. Shiraiwa, Biogeochemistry Department, Max Planck Institute for Chemistry, Becherweg 27/29, D-55128 Mainz, Germany.

N. Sugimoto, National Institute for Environmental Studies, Tsukuba 305-0053, Japan.

R. J. Weber, School of Earth and Atmospheric Sciences, Georgia Institute of Technology, Atlanta, GA 30332, USA.

Y. Zhao, Air Quality Research Center, University of California, One Shields Avenue, Davis, CA 95616, USA.